Crystal plasticity model for BCC iron atomistically informed by kinetics of correlated kinkpair nucleation on screw dislocation

Sankar Narayanan [a], David L. McDowell [a,b], Ting Zhu [a,b,*]

[a] *Woodruff School of Mechanical Engineering, Georgia Institute of Technology, Atlanta, GA 30332, USA*
[b] *School of Materials Science and Engineering, Georgia Institute of Technology, Atlanta, GA 30332, USA*

A R T I C L E   I N F O

A B S T R A C T

The mobility of dislocation in body-centered cubic (BCC) metals is controlled by the thermally activated nucleation of kinks along the dislocation core. By employing a recent interatomic potential and the Nudged Elastic Band method, we predict the atomistic saddle-point state of $1/2\langle 111 \rangle$ screw dislocation motion in BCC iron that involves the nucleation of *correlated* kinkpairs and the resulting double superkinks. This unique process leads to a single-humped minimum energy path that governs the one-step activation of a screw dislocation to move into the adjacent {110} Peierls valley, which contrasts with the double-humped energy path and the two-step transition predicted by other interatomic potentials. Based on transition state theory, we use the atomistically computed, stress-dependent kinkpair activation parameters to inform a coarse-grained crystal plasticity flow rule. Our atomistically-informed crystal plasticity model quantitatively predicts the orientation dependent stress–strain behavior of BCC iron single crystals in a manner that is consistent with experimental results. The predicted temperature and strain-rate dependencies of the yield stress agree with experimental results in the 200–350 K temperature regime, and are rationalized by the small activation volumes associated with the kinkpair-mediated motion of screw dislocations.

© 2014 Elsevier Ltd. All rights reserved.

1. Introduction

Plastic flow in body-centered cubic (BCC) metals is controlled by the motion of screw dislocations due to their high intrinsic lattice resistance (Argon, 2008; Vitek, 2008; Weinberger et al., 2013a). The resolved shear stress required to move a screw dislocation at 0 K (i.e., Peierls stress) is much higher than that for the edge dislocation, owing to the three-fold compact core of the former. However, this inherent difficulty to move a screw dislocation at finite temperatures can be mitigated by the thermal activation of kinks, which are essentially local perturbations on the straight dislocation line arising from the thermal fluctuation of atoms at the dislocation core. Hence, at finite temperatures (and low stresses) thermal activation of kinks is the rate-limiting step for the motion of screw dislocations in BCC metals (Seeger, 1956).

Thermally activated dislocation motion and its influence on the macroscopic plasticity of BCC crystals comprise a multiscale problem due to the extremely fine length and time scales of atomic vibration and the coarse scales of dislocation motion and interaction during plastic flow. Regarding the atomistic aspect of this problem, molecular statics studies have considered the Peierls stress for dislocation motion based on two-dimensional (2D) simulations (Chaussidon et al., 2006;

Chen et al., 2013; Groger et al., 2008a, 2008b; Koester et al., 2012). They also evaluated the material parameters quantifying the so-called non-Schmid effects on the Peierls Stress, i.e., the effect of (non-glide) stresses other than the maximum resolved shear stress (Bassani et al., 2001). However, these studies were limited to the 2D mode of dislocation motion at 0 K and could not account for the three-dimensional (3D) nature of the kinetics of dislocation motion via kink formation in the finite temperature regime.

Molecular dynamics (MD) studies have also been performed in the past with the aim of understanding the motion of screw dislocations for example in BCC Fe at finite temperatures (Chaussidon et al., 2006; Domain and Monnet, 2005; Gilbert et al., 2011). However, direct MD is limited in simulation of the kinetic dislocation motion owing to the rare event nature of thermally activated kink nucleation. Also, the stress levels predicted using MD are elevated due to the high strain rates, and it is implausible to use MD to predict the stress–strain behavior of typical laboratory experiments at low strain rates. These limitations of MD underscore the need for a coarse-grained approach that can predict mechanical behavior at longer time scales without sacrificing the richness of atomistic information to inform the rate-controlling mechanisms of dislocation motion.

One coarse-grained modeling approach involves computing activation parameters of unit processes of thermally activated dislocation motion and then using them to inform a crystal plasticity model by invoking transition state theory (Vineyard, 1957). In this scheme, the Nudged Elastic Band (NEB) method (Jonsson et al., 1998; Zhu and Li, 2010; Zhu et al., 2013) has been used to compute the activation parameters of kink nucleation along a screw dislocation in BCC metals (Gordon et al., 2010; Groger and Vitek, 2008; Ngan and Wen, 2002; Proville et al., 2012). For example, Groger and Vitek (2008) employed a periodically varying analytical Peierls potential for NEB studies of BCC Mo. Ngan and Wen (2002) used the NEB method and Embedded Atom Method (EAM) potential to study kink nucleation along the core of a screw dislocation in BCC Fe. They predicted a degenerate dislocation core that is inconsistent with the non-degenerate core predicted by newer EAM potentials (Gordon et al., 2011; Mendelev et al., 2003), Bond Order potential (Groger et al., 2008a) and Density Functional Theory (DFT) (Ventelon and Willaime, 2007). The EAM potential for Fe used in Gordon et al. (2010) yielded the metastable dislocation core and associated double-humped minimum energy path which are likely artifacts of the potential, based on comparison with more accurate DFT studies (Ventelon and Willaime, 2007; Weinberger et al., 2013b). Recently, Proville et al. developed an EAM potential (hereafter referred to as Proville-EAM) (Proville et al., 2012) that predicted a single-humped 2D energy barrier, which agrees with the DFT results.

In this work, we employ the Proville-EAM potential and NEB method to compute the stress-dependent activation parameters for the 3D mode of thermally activated screw dislocation motion. We find a single-humped reaction pathway (i.e., minimum energy path) that is physically manifested as a correlated process of nucleation of leading and trailing kinkpairs, each of which consists of two atomically discrete kinks. Such a composite kink structure arises from the discrete 3D nature of the saddle-point state of screw motion, in contrast to the conventional line tension model of kink nucleation (Seeger, 1956). The corresponding atomistic material parameters are used to inform a plastic flow rule by invoking transition state theory. This atomistically informed crystal plasticity model predicted the deformation behavior of BCC Fe single crystals, specifically for the experimentally relevant low stress and finite temperature regime, where kink activation is the rate-limiting step in the kinetics of screw dislocation motion. This departs from other atomistically informed crystal plasticity models for BCC crystals (Koester et al., 2012; Weinberger et al., 2012; Yalcinkaya et al., 2008) and other coarse-grained models (Patra and McDowell, 2012; Tang et al., 1998) that adopt an empirical relation (Kocks et al., 1975) for describing the energetics of kink nucleation as a function of stress. The predictions of the orientation dependent tensile stress–strain relation from our model are in good agreement with experimental results for a BCC Fe single crystal (Keh, 1965; Yalcinkaya et al., 2008), thus providing some measure of validation. Our model also predicts the temperature dependence of the yield stress, in quantitative agreement with the experimental results for BCC Fe (Kuramoto et al., 1979). The details of our atomistic methods and the crystal plasticity model are described in Section 2. The results and their implications are discussed in Sections 3 and 4, respectively. Concluding remarks are given in Section 5.

2. Computational methods

The atomistic Nudged Elastic Band method and the atomistically informed crystal plasticity model are described in detail in the following two subsections, respectively.

2.1. Atomistic modeling

The Nudged Elastic Band (NEB) method is capable of effectively determining the reaction pathway and activation parameters of a stress-driven, thermally activated process to enable application of transition state theory for dislocation kinetics (Zhu et al., 2005, 2007, 2008, 2004). In this work, we used the NEB method to compute the minimum energy path and associated activation energy of a unit process of dislocation slip via kink nucleation in BCC Fe single crystals. As briefly discussed in the Introduction, the widely-used EAM potential developed by Mendelev et al. (2003) is a favorable candidate for the atomistic simulations, since it well predicts the properties and also predicts a non-degenerate core for the screw dislocation, unlike its predecessors which had predicted a degenerate core structure (Ackland et al., 1997; Johnson and Oh, 1989). However, this potential predicts a double-humped 2D Peierls barrier with a metastable minimum, which is inconsistent with the single-humped Peierls barrier predicted by DFT (Ventelon and Willaime, 2007; Weinberger et al., 2013b). The most
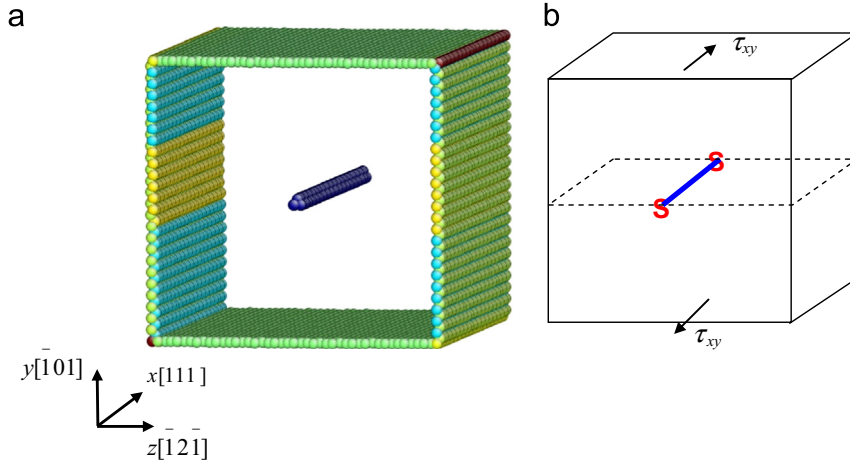
Fig. 1. Atomistic simulation set-up. (a) 3D perspective view of the supercell and the dislocation at its initial energy minimum state colored by centro-symmetry parameter (Li, 2003). (b) Schematic of the supercell showing details of the loading scheme.

recent version of the Mendelev-EAM potential (Gordon et al., 2011) also predicts a double-humped barrier, although the depth of the metastable valley is less pronounced than its earlier version. Recently, Proville et al. (2012) developed an EAM potential that predicted a single-humped Peierls barrier with an activation energy close to that predicted by DFT. Hence, we use the Proville-EAM potential for carrying out the atomistic simulations aimed at obtaining the mechanistically-based material parameters for the crystal plasticity model.

Fig. 1(a) shows the 3D simulation supercell embedded with a screw dislocation at its ground state. The x, y and z axes are respectively oriented along the $[111]$, $[\bar{1}01]$ and $[\bar{1}2\bar{1}]$ directions. The simulation supercell is 54 nm long along its out-of-plane $[111]$ direction and its in-plane dimensions are 25 nm and 25 nm, respectively. For the 2D molecular statics calculations of the Peierls stress, we used the same setup but with a reduced out-of-plane dimension of 12.5 nm. The 1/2 $[111]$ screw dislocation is created at the center of the supercell by superimposing its elastic displacement field and subsequently relaxing the supercell with conjugate gradient method to obtain the minimum energy state. The outermost $(\bar{1}01)$ and $(\bar{1}2\bar{1})$ planes constituting the in-plane boundaries are traction free and hence fully relaxed so as to avoid the effect of stresses perpendicular to the glide direction. The shear stress required to move the dislocation is exerted by imposing a displacement-controlled boundary condition on a thin boundary layer of $(\bar{1}01)$ face, while the bottom boundary layer is held fixed. The dislocation glides on the maximum resolved shear stress plane (MRSSP), which is the $(\bar{1}01)$ plane for our setup. In this paper, all the atomic configurations are colored by the centro-symmetry parameter (Li, 2003) for showing the core structure of the screw dislocation.

NEB calculations were performed using the parallel molecular dynamics simulator LAMMPS (Plimpton, 1995). Results were verified using an in-house NEB code. The initial state of the screw dislocation in the NEB simulation is shown in Fig. 1(a), and the final state is the energy minimum state of the same dislocation moved by one atomic distance from its initial state into the adjacent {110} Peierls valley. The intermediate replicas are generated by linearly interpolating between atomic coordinates of the initial and final states. All the replicas are interconnected with springs that exert inter-replica forces, so as to rearrange replicas equi-distantly along the minimum energy path. The climbing image algorithm (Henkelman et al., 2000) is used to locate the saddle point of the energy barrier. The results were found to be insensitive to the value of the spring constant. A force tolerance of 0.05 eV/Å is employed to check the convergence of the NEB simulation.

2.2. Atomistically informed crystal plasticity modeling

We employ the crystal plasticity model structure of Asaro and Needleman (1985) and Kalidindi et al. (1992) to study the elastic-viscoplastic behavior of BCC Fe single crystals. In the continuum mechanics framework of finite deformation, the deformation gradient tensor $\mathbf{F}$ is decomposed as $\mathbf{F} = \mathbf{F}^*\mathbf{F}_p$, where $\mathbf{F}^*$ and $\mathbf{F}_p$ are the elastic and plastic deformation gradients, respectively. The time rate of the plastic deformation gradient is given by

$$\dot{\mathbf{F}}_p = \mathbf{L}_p \mathbf{F}_p \tag{1}$$

where

$$\mathbf{L}_p = \sum_\alpha \dot{\gamma}^\alpha \mathbf{S}_0^\alpha \tag{2}$$

is the plastic deformation velocity gradient and $\mathbf{S}_0^\alpha = \mathbf{m}_0^\alpha \otimes \mathbf{n}_0^\alpha$, where $\mathbf{m}_0^\alpha$ and $\mathbf{n}_0^\alpha$ are fixed orthonormal unit vectors, defining respectively the slip direction and slip plane normal of the {110}⟨111⟩ slip system α in the reference configuration. Here, $\dot{\gamma}^\alpha$ is the plastic shearing rate on slip system α, given by Orowan's relation $\dot{\gamma}^\alpha = b\rho v^\alpha$, where b is the Burgers vector length of the

screw dislocation, ρ is the mobile dislocation density, and v^α is the dislocation velocity on slip system α. Using transition state theory, the flow rule for $\dot{\gamma}^\alpha$ is related to the stress-biased activation energy for dislocation motion, i.e.,

$$v^\alpha = v_0 \exp\left(-\frac{H(\tau_{\text{eff}}^\alpha)}{k_B T}\right) \tag{3}$$

where v_0 is the reference dislocation velocity, H is the activation energy for unit dislocation slip, k_B is the Boltzmann constant, T is the absolute temperature, and τ_{eff}^α is the effective shear stress that drives dislocation motion on slip system α. Since kink nucleation is the rate-limiting step for screw dislocation motion, it controls the kinetics in Eq. (3) via dependence on the associated activation energy H, as discussed later. Combining the Orowan relation with Eq. (3) leads to

$$\dot{\gamma}^\alpha = \begin{cases} 0, & \text{if} \quad \tau_{\text{eff}}^\alpha \leq 0 \\ \dot{\gamma}_0 \exp\left(-\frac{H(\tau_{\text{eff}}^\alpha)}{k_B T}\right) \text{sign}(\tau^\alpha), & \text{if} \quad \tau_{\text{eff}}^\alpha > 0 \end{cases} \tag{4}$$

where the pre-factor $\dot{\gamma}_0$ is the reference strain rate. The effective resolved shear stress τ_{eff}^α on slip system α is expressed as the difference between the applied resolved shear stress and the athermal slip resistance s_a^α due to the long-range barriers, i.e.,

$$\tau_{\text{eff}}^\alpha = |\tau^\alpha| - s_a^\alpha \tag{5}$$

Based on the assumption that elastic stretch is infinitesimal for metals, τ^α can be expressed as

$$\tau^\alpha = (\mathbf{C}^*\mathbf{T}^*) : \mathbf{S}_0^\alpha \approx \mathbf{T}^* : \mathbf{S}_0^\alpha \tag{6}$$

where $\mathbf{C}^*$ is the right Cauchy-Green tensor given by $\mathbf{C}^* = \mathbf{F}^{*T}\mathbf{F}^*$ and $\mathbf{T}^*$ is the second Piola–Kirchhoff stress tensor (Kalidindi et al., 1992).

The stress-dependant kink activation energy H in Eq. (4) can be written in the Kocks form (Kocks et al., 1975) as

$$H = H_0 \left[1 - \left(\frac{\tau_{\text{eff}}^\alpha}{s_{t0}}\right)^p\right]^q \tag{7}$$

where H_0 is the activation energy for dislocation motion when the effective shear stress τ_{eff}^α is zero, p and q are the profiling parameters, and s_{t0} is the thermal slip resistance at 0 K (Peierls stress), assuming the same value for all the slip systems $s_{t0}^\alpha \approx s_{t0}$ (Kothari and Anand, 1998). Since the thermal part of the slip resistance in BCC metals is primarily due to the lattice resistance that does not evolve with deformation, we treat s_{t0} as a constant. Thus, the part of the total slip resistance that evolves is the athermal slip resistance s_a^α due to the long-range barriers. The evolution of s_a^α, with the same initial value for all the slip systems $s_{a0}^\alpha \approx s_{a0}$ (Kothari and Anand, 1998), is prescribed as

$$\dot{s}_a^\alpha = \sum_\beta q^{\alpha\beta} h^\beta |\dot{\gamma}^\beta| \tag{8}$$

where $q^{\alpha\beta}$ is the hardening matrix (Asaro and Needleman, 1985) given by $q^{\alpha\beta} = Q + (1-Q)\delta_{\alpha\beta}$ (Q is the latent hardening coefficient and $\delta_{\alpha\beta}$ is the Kronecker delta), and h^β is the self-hardening rate of slip system β given as

$$h^\beta = h_0 \left(1 - \frac{s_a^\beta}{s_{a,s}^\beta}\right)^r \text{sign}\left(1 - \frac{s_a^\beta}{s_{a,s}^\beta}\right) \tag{9}$$

where h_0 is the initial self-hardening rate, r is a material parameter and $s_{a,s}^\beta$ is the saturation value of the athermal slip resistance.

The crystal plasticity model illustrated to this point is the standard approach. We next explain how information regarding the unit process of kink nucleation from the atomistic model is bridged with the crystal plasticity model. The atomistic NEB calculation (as explained in Section 2.1) enables the quantification of kinkpair activation energy H as a function of the effective applied shear stress τ_{eff}^α. The atomistically computed data for H versus τ_{eff}^α are then fit to the Kocks form as in Eq. (7). Thus, the values of the parameters H_0, p, q and s_{t0} in Eq. (7) are determined from our atomistic results.

The pre-exponential factor $\dot{\gamma}_0$ in Eq. (4) is also atomistically informed and estimated as follows. Assuming that the Debye frequency ν_D for BCC Fe can be used as a quantitative measure for the attempt frequency of nucleation of thermal kinks, $\dot{\gamma}_0$ can be approximately written as (Groger and Vitek, 2008)

$$\dot{\gamma}_0 = \frac{b^2 a \rho \nu_D}{l} \tag{10}$$

where l is the lateral extent of kinks at the saddle-point state and a is the distance that the dislocation moves in one activation step, equal to the lattice constant in the $[\bar{1}2\bar{1}]$ direction. The value of l can be estimated from our atomistic results and thus $\dot{\gamma}_0$ becomes an atomistically informed property for a given mobile dislocation density.

We choose to consider only the twelve {110}⟨111⟩ slip systems in our crystal plasticity model and exclude the twelve {112}⟨111⟩ slip systems. This is because we have found in our atomistic studies that each unit process of slip in a {112} plane proceeds by two individual slip steps on the non-parallel {110} planes. As a result, the rate-limiting step for slip on a {112}⟨111⟩ slip system is still the formation of kinks on the {110}⟨111⟩ slip system that is studied in this work. However, in the case of the MRSSP close to {112} (wavy slip on {112} has been often observed at finite temperatures in BCC metals (Seeger, 2001)), our viscoplastic formulation can effectively approximate the kinematic effect of plastic shear on the

{112}⟨111⟩ slip system through simultaneous activation of the most highly stressed primary slip system of {110}⟨111⟩ and other less stressed ones. In addition, experimentally observed finite temperature cross slip into any crystallographic plane between the primary and secondary {110}⟨111⟩ slip systems can also be activated depending on the ratio of the number of elementary steps on the primary and the secondary {110}⟨111⟩ planes. The simultaneous activation of multiple {110}⟨111⟩ systems is facilitated by the relatively small activation volume of screw dislocation motion in BCC metals and accordingly large strain rate sensitivity, to be detailed later.

3. Results

3.1. Molecular statics and 2D NEB

We performed several benchmark calculations to verify that the Proville-EAM predicts the correct features of BCC Fe apart from the basic crystalline properties verified in Proville et al. (2012). Fig. 2 shows the differential displacement plot of a screw dislocation core (Vitek, 2004) as predicted by Proville-EAM based on a conjugate gradient energy minimization calculation. The core spreads onto the three {110} planes of the [111] zone and is non-degenerate, as it does not exhibit dyadic asymmetry. The non-degeneracy of the core is in accordance with the DFT results (Ventelon and Willaime, 2007; Weinberger et al., 2013b). We also evaluated the 0 K Peierls stress as a function of the orientation of the MRSSP, using a conjugate gradient energy minimization loading scheme. Anti-plane shear was applied onto a 2D simulation cell, which corresponds to the 3D simulation cell in Fig. 1 with reduced thickness. The incremental displacement was imposed on a boundary layer of the ($\bar{1}$01) plane, with energy minimization carried out after each increment. The magnitude of the
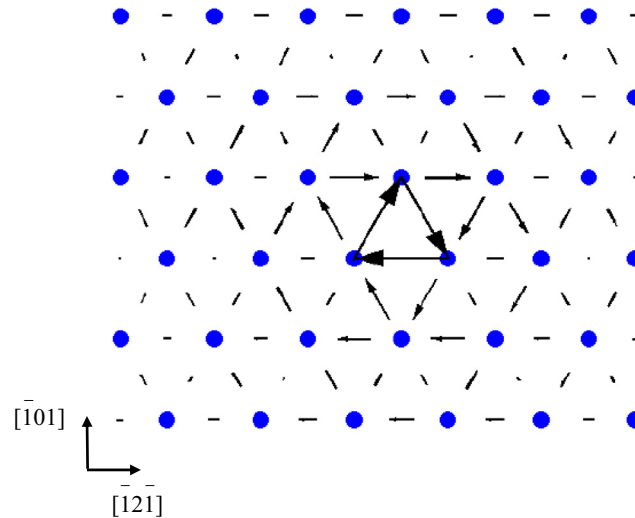

Fig. 2. Differential displacement plot of the non-degenerate screw dislocation core predicted by Proville-EAM.
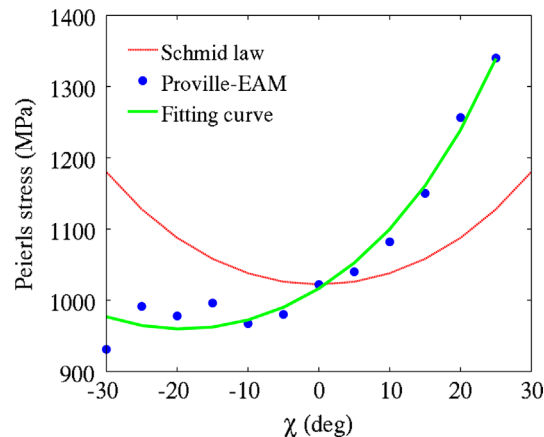

Fig. 3. Orientation dependence of the Peierls stress predicted by Proville-EAM in 2D simulations. The results are fit to an equation of the form (Groger et al., 2008b) CRSS(χ) = τ_{cr}^*[cos χ + a_1 cos(χ + π/3)] and the values of the fitting parameters are $a_1 = 0.50$ and $\tau_{cr}^* = 1.27$ GPa.
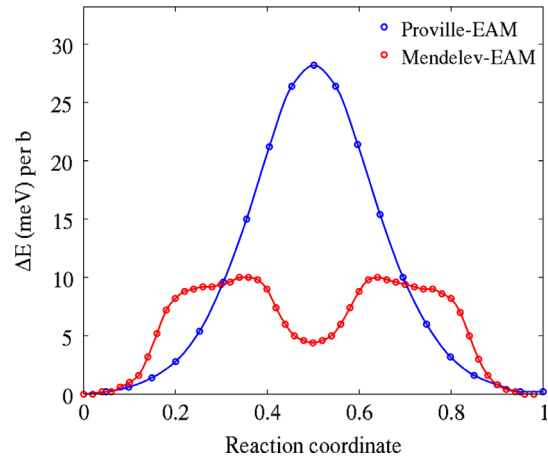
Fig. 4. 2D Peierls barriers predicted by Proville-EAM and Mendelev-EAM potentials.

incremental displacement was controlled to limit the build-up of stress to $0.001C_{44}$, where C_{44} is the elastic constant of BCC Fe. To evaluate the orientation effect on MRSSP, new configurations were created by rotating the simulation cell about the [111] axis in Fig. 1 by an angle χ, whose magnitude is between $-30°$ and $+30°$ owing to the symmetry of the BCC lattice. As shown in Fig. 3, the orientation dependent Peierls stress does not follow Schmid's law and instead exhibits an asymmetry which is due to the twinning–antitwinning asymmetry intrinsic to the BCC lattice (Chaussidon et al., 2006; Groger et al., 2008a).

We also conducted 2D NEB calculations of the energy barrier for the screw dislocation motion, in order to compare different EAM potentials. While the physically meaningful energy barriers require 3D NEB calculations, the 2D NEB study can be readily compared with the computationally intensive DFT results, thereby providing a quick check regarding the quality of EAM potentials. The 2D NEB result from Proville-EAM is compared with that predicted by Mendelev-EAM in Fig. 4. The Proville-EAM predicts a single-humped curve, while the Mendelev-EAM predicts a double-humped one with a metastable intermediate state, as discussed earlier. The saddle-point energy of 0.028 eV per b from Proville-EAM is comparable to that from DFT (Proville et al., 2012).

These results show that the Proville-EAM can effectively describe dislocations in BCC Fe. However, since these 2D calculations cannot capture the 3D localized mode of kink nucleation as the rate-limiting step of screw dislocation motion, we proceed next with 3D NEB simulations.

3.2. Correlated kinkpair nucleation

3D NEB simulations were carried out with the simulation setup in Fig. 1 to study the mechanism of kink nucleation and obtain the stress-dependent activation parameters. Fig. 5(a) shows a converged minimum energy path for the unit process of thermally activated screw dislocation glide under zero applied stress, in which the energy of replicas is plotted against the reaction coordinate defined as the normalized path length of minimum energy path. The atomic configurations of replicas are shown in Fig. 5(b). Replicas 1 and 19 are respectively the initial and final states of the unit process, where the core of the screw dislocation moves by one atomic distance on the $(\bar{1}01)$ plane, along the $[\bar{1}2\bar{1}]$ direction. The rest of the configurations are those of intermediate replicas on the minimum energy path. The saddle-point state is replica 7 and it has an energy of 0.57 eV, assuming the initial state has zero energy. It can be seen that the dislocation moves one atomic distance by the nucleation of four different kinks, K1, K2, K3 and K4, as marked in the replicas of Fig. 5(b). K1 and K2 are hereby defined as the *leading kinks* and together form the *leading kinkpair*, while K3 and K4 are defined as the *trailing kinks* and together form the *trailing kinkpair*, the reasons for which are discussed below.

To understand the crystallographic details of the kinkpair nucleation, it is important to first understand the structural changes of the dislocation core due to the nucleation of the kinkpairs. For that purpose, we plot the differential displacement (DD) maps of various points along the dislocation line at its saddle state (replica #7 of Fig. 5(b)). The results are shown in Fig. 6. Fig. 6(b–f) are the DD plots of the cross-sections (with [111] as their normals) as marked on the saddle state of Fig. 6(a). The four individual kinks are also marked. The three {110} planes of the [111] zone are marked in Fig. 6(b). Fig. 6(b) shows the non-degenerate compact core of the part of the dislocation in the initial Peierls valley, P1, marked as point (b). As can be noted, the core is compact and spread equally into the three {110} planes. Point (c) on the dislocation line denotes the local core spreading due to the first leading kink, K1. The corresponding DD plot shows that the core is spread along the $(\bar{1}01)$ plane. Fig. 6(f) shows the compact core state of the part of the dislocation line in the new Peierls valley, P2; and Fig. 6(d–e) show the rest of the split core states between the two compact core states. Thus, the compact core states in the adjacent Peierls valleys (points (b) and (f)) are progressively bridged by the split-core states of points (c), (d) and (e) which in total involve the four atomistically discrete kinks, i.e., K1–K2 (leading kinkpair) and K3–K4 (trailing kinkpair). Meanwhile, the saddle state predicted by Mendelev-EAM has a split-core state that is uniformly the same along
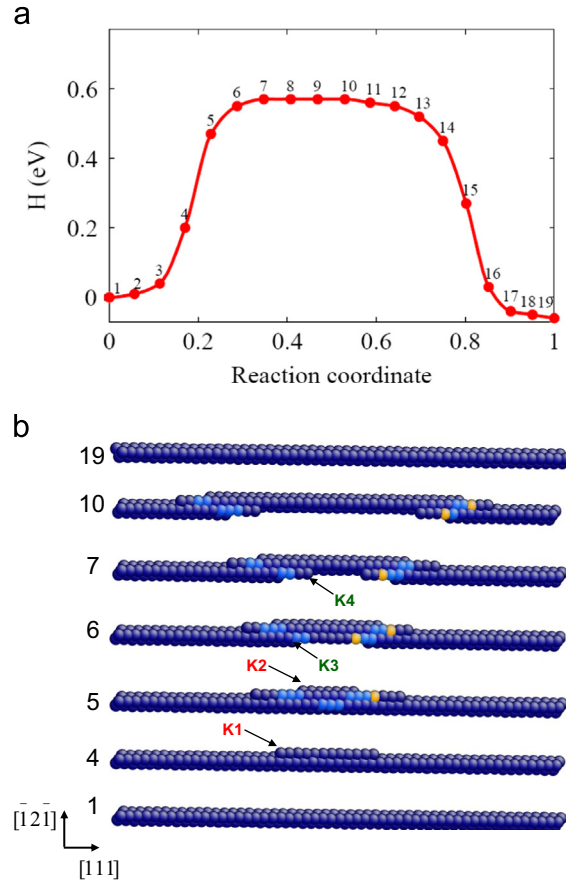
Fig. 5. 3D NEB results of thermally activated screw dislocation motion at zero stress. (a) Minimum energy path for the correlated kinkpair nucleation. (b) Atomic configurations of the corresponding replicas along the minimum energy path.

the dislocation line, as seen in replica #11 of Fig. A1(b) in Appendix A. The DD plot of its core structure in Fig. A1(c) is comparable to the short split-core segment represented by point (d) in the saddle state of Fig. 6(a).

The salient feature of our 3D NEB result is the activation mechanism of *correlated* kinkpair nucleation, which results in a single-humped minimum energy path unlike the Mendelev-EAM that predicts a double-humped one (Gordon et al., 2010), as shown in Appendix A. Fig. 7(a) shows a perspective view of the saddle-point state (replica 7 in Fig. 5(b)) colored based on centro-symmetry parameter, and its crystallographic details, as understood from Figs. 6 and 7(a) are shown in the schematic of Fig. 7(b). The kinks K1 and K2 (leading kinkpair) nucleate first and are colored in red, while the kinks K3 and K4 (trailing kinkpair) nucleate subsequently, and are colored in green. Thus the saddle-point state is composed of both the leading and the trailing kinkpairs, unlike the split-core saddle state predicted by Mendelev-EAM (see Fig. A1(b)). Such a nucleation event, in which both the leading and trailing kinkpairs nucleate simultaneously, can be considered as a correlated mode (Gordon et al., 2010) and accordingly referred to as 'correlated kinkpair nucleation'. It can be observed that the correlated kinkpair nucleation involves two adjacent ($\bar{1}01$) planes. In Fig. 7(b), the top ($\bar{1}01$) plane and the kinks within this plane are represented by solid lines, while the bottom plane and its kinks by dotted lines. The leading kink K2 and the trailing kink K3, lie on the top ($\bar{1}01$) plane and shift the two atomic columns on the top ($\bar{1}01$) plane by one lattice distance, while the leading kink K1 and the trailing kink K4 lie on the bottom ($\bar{1}01$) plane and shift the bottom column by one lattice distance, which together translate the dislocation line into the new Peierls valley, P2. Hence, a single event of correlated kinkpair nucleation involves the coordinated movement of kinks on two ($\bar{1}01$) planes of the [111] zone.

The leading and trailing kinkpairs are collectively defined as one *superkink*, marked as SK1 in Fig. 7(a). The prefix 'super' emphasizes the composite nature of each superkink, composed of four constituting kinks. Incidentally, the superkink should not be confused with a kink traversing several lattice valleys, which has been termed as a 'macro-kink' (Caillard, 2010). Note that the nucleation event of an opposite superkink occurs simultaneously and is marked as SK2 in Fig. 7(a). As a result, the saddle-point configuration involves the *double superkinks* of opposite signs, and each superkink consists of both leading and trailing kinkpairs.

The formation of *double superkinks* produces a localized displacement of the screw dislocation from the Peierls valley P1–P2 on the ($\bar{1}01$) plane via a one-step transition, as shown in Fig. 7(b). This unique one-step transition and its single-humped activation pathway contrast with the two-step transition and the associated double-humped activation pathway
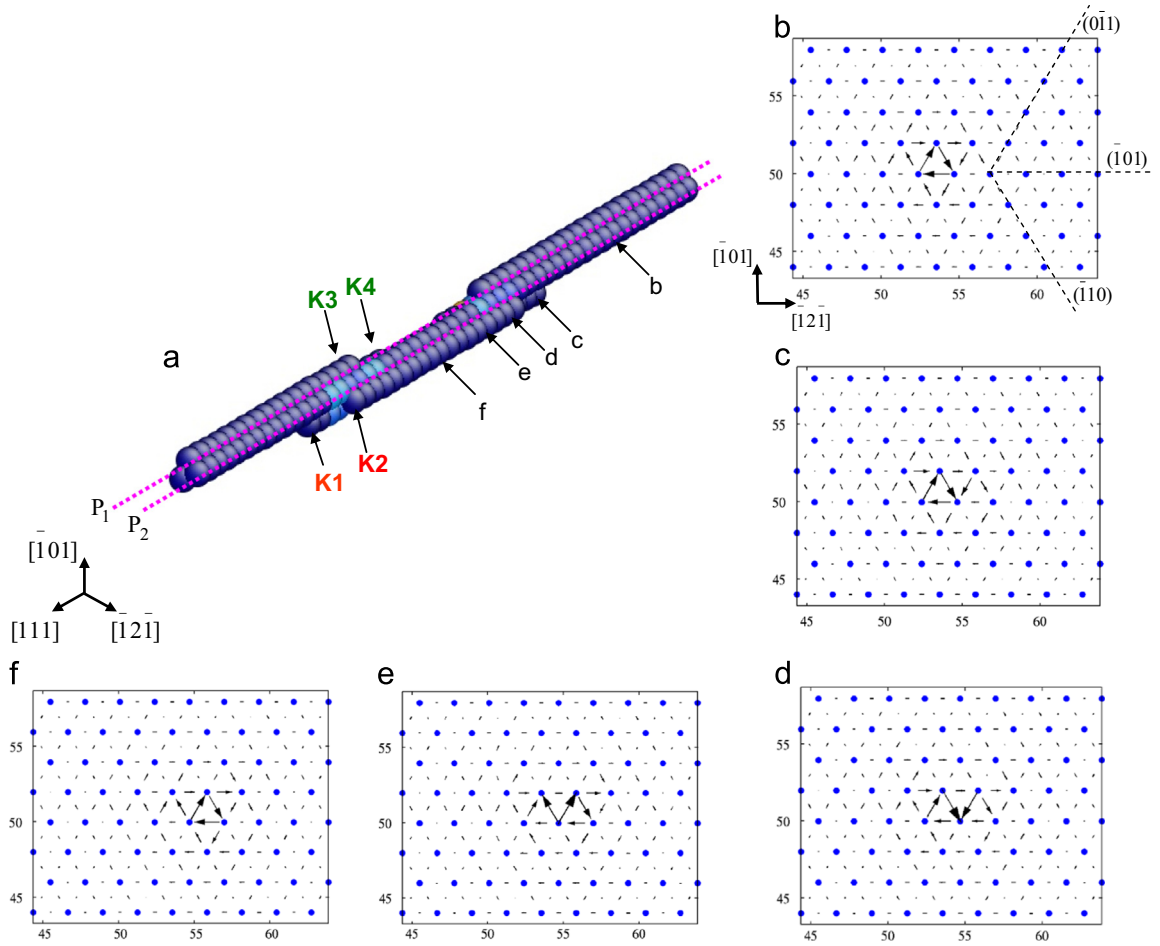
Fig. 6. Differential displacement (DD) plots for the saddle-point state (replica #7 of Fig. 5(b)). (a) Atomic structure of the dislocation core at the saddle state. (b–d) Corresponding DD plots at various points along the dislocation core, as marked in Fig. 6(a). The unit of x–y axes is angstrom.

predicted by other interatomic potentials, e.g., Fig. A1(a) in Appendix A. This will be further addressed in the Discussion section. The distance between the leading kinks K1 in the double-superkink structure at the saddle point corresponds to the value for l in Eq. (10) for determining the pre-factor $\dot{\gamma}_0$ and is characteristically around $25b$.

3.3. Stress-dependent kinkpair activation energy and activation volume

We repeated NEB calculations for varying levels of applied shear stress to characterize the stress dependence of the activation energy for correlated nucleation of kinkpairs (i.e., double superkinks of opposite signs). The initial and final states for the NEB calculation were maintained at similar shear-stress levels by holding constant the finite-displacement of the surface layer. Fig. 8(a) shows the minimum energy paths for various applied shear stresses. As the shear stress is increased, the minimum energy path is tilted and the saddle-point energy is reduced accordingly. At an applied shear stress around 1.04 GPa, the energy barrier vanishes, which implies that the kinkpair nucleation occurs spontaneously at this stress level without the need for overcoming a barrier by thermal activation. This stress value should thus correspond to the classical Peierls stress at 0 K, which is conventionally used as a quantitative measure for the intrinsic lattice resistance to dislocation motion. Our 2D simulation results shown in Fig. 2 also predicted the same magnitude for the Peierls stress (for $\chi = 0$), which thus serves as a check for the 3D NEB implementation and results. Incidentally, the minimum energy paths in Fig. 8(a) are similar to those reported by Proville et al. (2012). However, they did not study the atomic details of the activation mode and did not consider their implications for crystal plasticity modeling.

Fig. 8(b) shows the activation energy H as a function of the applied shear stress, which is denoted as τ_{eff}^α in our crystal plasticity model. The data points in the plot of H versus τ_{eff}^α can be fit to Eq. (7) to obtain the material parameters for quantifying the kinkpair nucleation kinetics. The activation energy for dislocation motion at zero stress, H_0, is the intercept of the H versus τ_{eff}^α curve on the y-axis, given by 0.57 eV. The thermal slip resistance at 0 K, s_{t0}, is the intercept on the x-axis, given by 1.04 GPa. They will be further discussed later. The dimensionless profiling parameters, p and q, are 0.667 and 1.18,
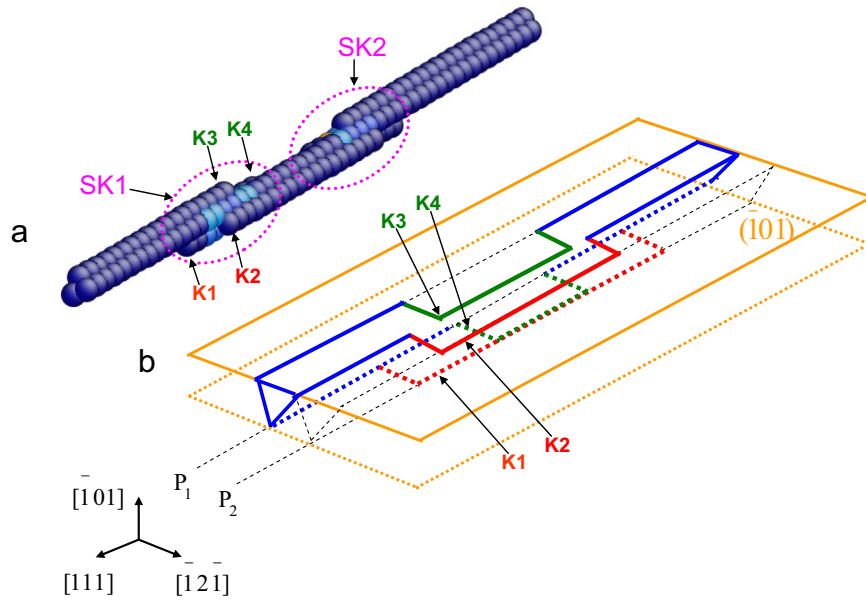
Fig. 7. Atomistic details of correlated kinkpair nucleation. (a) Perspective view of the saddle point state showing the double superkink, SK1 and SK2, as well as the constitutive individual kinks, K1–K4. (b) Schematic showing the crystallographic details of the saddle-point configuration. P_1 and P_2 indicate the adjacent Peierls valleys. Note that the top ($\bar{1}01$) plane and the kinks within this plane are represented by solid lines, while the bottom plane and its kinks are represented by dotted lines.
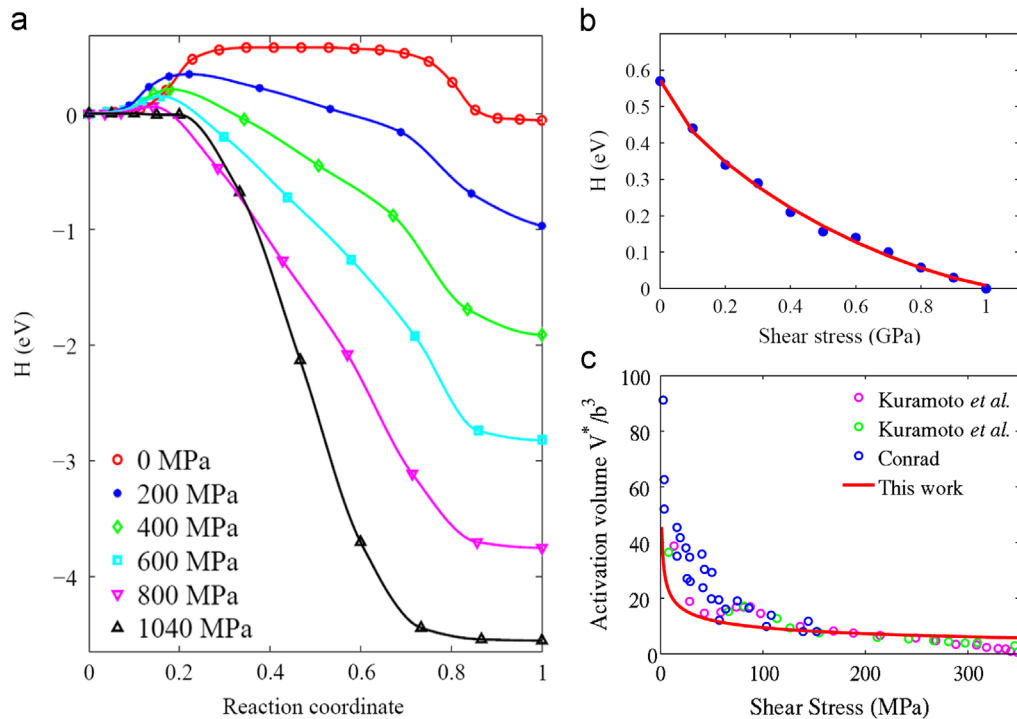
Fig. 8. Shear stress-dependent minimum energy path (MEP) and activation energy. (a) MEPs for correlated kinkpair nucleation at different shear stresses. (b) Data points of calculated activation energy versus shear stress, fit to a curve of the Kocks form as in Eq. (7). (c) Calculated activation volume as a function of shear stress, compared with experimental measurements by Kuramoto et al. (1979) and Conrad (1960).

respectively. These atomistically determined values are numerically close to $p = 0.748$ and $q = 1.172$, derived by Tang et al. (1998) by fitting to the experimental results for BCC Ta. But our values of p and q differ significantly from the ones customarily assumed in crystal plasticity models, e.g., $p = 1$ and $q = 2$ as in Koester et al. (2012), $p = 1$ and $q = 1$ as in

Table 1
Atomistically determined parameters for stress-dependent activation energy H and shearing rate prefactor $\dot{\gamma}_0$.

H_0	s_{t0}	p	q	$\dot{\gamma}_0$
0.57 eV	1.04 GPa	0.67	1.18	$3.19 \times 10^7/s$

Table 2
Material parameters for the crystal plasticity model.

$s_{a0}(=s_{a0}^{\alpha})$	h_0	Q	r	$s_{a,s}(=s_{a,s}^{\alpha})$
18 MPa	500 MPa	1.4	1.8	160 MPa

Yalcinkaya et al. (2008). To evaluate $\dot{\gamma}_0$ in Eq. (10), we first estimate the Debye frequency for Fe according to Hill (1986).

$$v_D = \left(\frac{3N}{4\pi V}\right)^{1/3} v_s \tag{11}$$

where N/V is the number density of the BCC lattice (0.0846 Å^{-3}) and v_s is the speed of sound, which is equal to 5130 m/s in Fe. The value of v_D is thus estimated to be 1.39×10^{13}/s. The dislocation density is assigned as 10^{15}/m^2, which is a reasonable value for plastically deformed crystals at moderate levels of deformation. As discussed earlier, the value of l is characteristically about $25b$, corresponding to the length between the two superkinks at the saddle state in NEB results. The value of a is numerically equal to the lattice constant in the $[\bar{1}2\bar{1}]$ direction, which is 2.298 Å. Given all these values, Eq. (10) yields $\dot{\gamma}_0 = 3.19 \times 10^7/s$. The values of the above atomistically determined material parameters are listed in Table 1.

The stress-dependant activation volume, V^*, for the nucleation of double superkinks can be estimated from the slope of the H versus $\tau_{\text{eff}}^{\alpha}$ curve, as it is defined as $V^* = -\partial H(\tau_{\text{eff}}^{\alpha})/\partial \tau_{\text{eff}}^{\alpha}$. Note that the activation volume is a function of stress, as shown in Fig. 8(c), and decreases as stress is increased, which correlates well with the experimental estimates from the strain-rate sensitivity measurements (Conrad, 1960; Kuramoto et al., 1979). For stresses greater than 0.2 GPa, the activation volume varies slowly between about $2b^3$ and $7b^3$. Below 0.2 GPa, the activation volume starts increasing at a faster rate, since the rate of change of the slope of the H versus $\tau_{\text{eff}}^{\alpha}$ curve is larger in this regime. Overall, the computed activation volume is small, in the range of 1–$20b^3$. These characteristically small activation volumes are expected, since the nucleation of double superkinks is a highly localized mode of displacement of the dislocation core, occurring over a length scale of a few nanometers. The small activation volumes could lead to significant temperature and strain rate sensitivity of the yield stress (Zhu et al., 2008), as shown next.
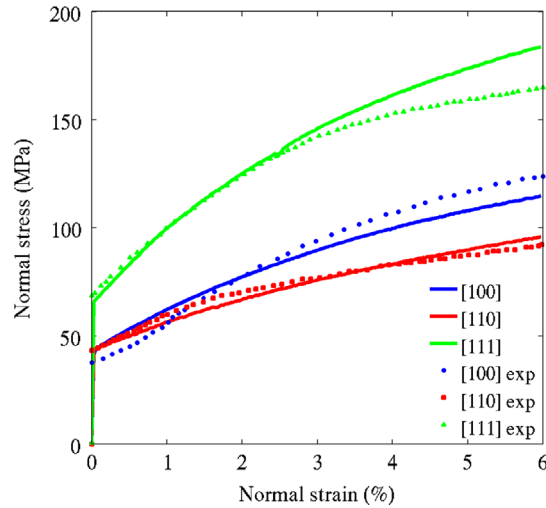
3.4. Stress–strain behavior from crystal plasticity simulations

The atomistically determined material parameters in Table 1 are introduced into our crystal plasticity model, so as to enable the atomistically informed simulation of uniaxial tensile tests of BCC Fe single crystals. In this work, we focus on the orientation, temperature and strain rate dependence of the yielding and hardening behavior. The elastic constants for BCC Fe are set to $C_{11}=236$ GPa, $C_{12}=134$ GPa, and $C_{44}=119$ GPa (Koester et al., 2012; Yalcinkaya et al., 2008). Table 2 lists the values of all other material parameters in our model, apart from the atomistically determined ones in Table 1. Essentially, the parameters in Table 2 characterize the work hardening behavior rather than initial yield stress. Simulation results are compared with experimental results for BCC Fe single crystals (Keh, 1965). The strain rate employed in our crystal plasticity simulations was $3.3 \times 10^{-4}/s$, consistent with the strain rate used in the aforementioned experiments.

Fig. 9 shows the stress–strain curve of uniaxial tension for three different orientations, i.e., [100], [110] and [111], compared with their corresponding experimental curves. It is noted that our atomistic results predict the temperature and rate dependent flow, while the work hardening is a result of correlation of the overall dataset of model parameters. The atomistically informed crystal plasticity model exhibits a strong orientation dependence of initial yield stress and work hardening that matches the corresponding experimental data reasonably well. Such orientation dependence can be qualitatively understood in terms of the Schmid factors. Namely, the orientation difference between the applied load and the primary slip system is mainly responsible for the difference of the tensile stress at the yield point.

Fig. 10(a) and (b) shows the tensile stress–strain curves predicted by the atomistically informed crystal plasticity model for various temperatures and strain rates, for the [100] loading orientation. The results show that the plastic behavior of BCC Fe single crystals depends strongly on temperature and strain rate, which is understandable considering the small activation volumes (1–$20b^3$) associated with the localized nucleation of kinkpairs and the small distance between the two superkinks. The strain rate dependent yield stresses in Fig. 10(b) are used to calculate the rate sensitivity parameter m according to $m = \partial \ln \tau_{\text{eff}}^{\alpha}/\partial \ln \dot{\gamma}^{\alpha}$, giving $m = 0.05$. This value falls within the range of experimentally determined values for BCC Fe of various grain sizes, as reported by Wei et al. (2004).

The yield stress from our crystal plasticity simulations is extracted as a function of temperature for the [100] loading orientation and is compared in Fig. 11 with the experimental results by Kuramoto et al. (1979) and Brunner and Diehl (1991).

Fig. 9. Orientation dependent stress–strain behavior of BCC Fe predicted by our atomistically informed crystal plasticity model, compared with experimental stress–strain curves (Keh, 1965).
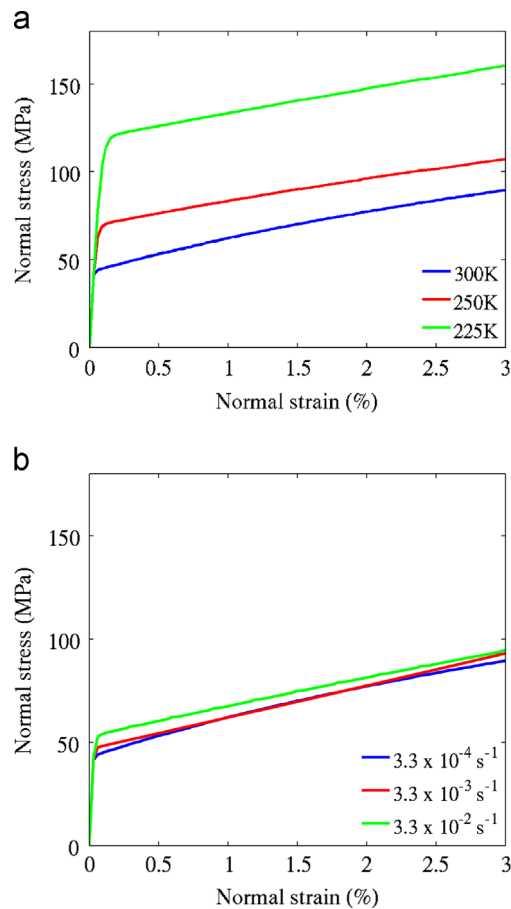
Fig. 10. Predictions from our atomistically informed crystal plasticity model for tensile loading along the [100] orientation. (a) Temperature dependence of stress–strain behavior at a strain rate of 3.3×10^{-4}/s. (b) Strain rate dependence of stress–strain behavior at 300 K.

The yield stress predictions match very well with those by experiments for the temperature range 200–350 K, which is of our interest in this work. Below 200 K, we find that the yield stress predictions by our model are higher than the experimental values and lack quantitative agreement. This discrepancy is expected, considering the high values of the Peierls stress predicted by the EAM potentials in general which are around 2–3 times the experimentally observed yield
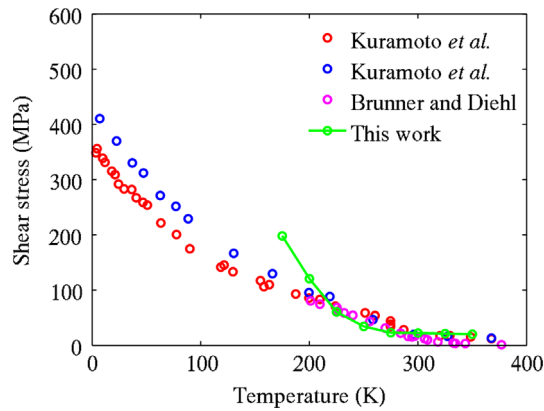
Fig. 11. Yield stress as a function of temperature for the [100] loading orientation: comparing crystal plasticity results with experimental results from Kuramoto et al. (1979) and Brunner and Diehl (1991).

stresses at finite temperatures, extrapolated to 0 K. Such inconsistency between the atomistic and experimental predictions of yield stresses has been well discussed in the literature. However, it is not fully resolved yet, even though various explanations such as the quantum effect (Proville et al., 2012; Suzuki, 1968), effect of interaction between a group of dislocations (Groger and Vitek, 2007), role of mixed dislocations in controlling the yield (Kang et al., 2012), etc. have been suggested in the past. Irrespective of this unresolved issue, our study proves that kinkpair activation parameters obtained from NEB calculations can be successfully incorporated into a crystal plasticity model to predict the macroscopic stress–strain behavior at low stresses in the regime around room temperature.

4. Discussion

In this section we discuss the implications of our atomistic results regarding kinkpair nucleation, as well as the assumptions made in our atomistic and crystal plasticity models, and their linkage. First, we emphasize that the mechanism of *correlated* kinkpair nucleation revealed in our atomistic simulations is a direct outcome of the single hump of the energy barrier predicted by Proville-EAM. We observed that the correlated kinkpair nucleation occurred at all levels of applied shear stress (below the Peierls stress). This observation contrasts with the approach of Gordon et al. (2010) who achieved the correlated mode (while employing the Mendelev-EAM) by tailoring the atomic configurations of the correlated mode. However, they were able to realize the correlated mode only for very low shear stress levels; above a threshold value of 80 MPa, the correlated mode spontaneously transformed to the uncorrelated mode, due to the double-humped energy barrier predicted by the Mendelev-EAM potential.

The atomistic details illustrated in Figs. 5–7 clearly show the correlated kinkpair nucleation and the resulting thermal activation of screw dislocation motion by double superkinks. These results enrich the classical picture of double-kink nucleation, which is supposed to be comprised of only two separated individual kinks (of opposite signs) activated on the glide plane, an example for which is the double kinks formed in Si (Bulatov et al., 1995). In the case of BCC Fe, the compact screw dislocation core is spread into the three {110} planes of the [111] zone, involving three [111] columns of atoms. Hence, a unit process of dislocation motion crystallographically necessitates the formation of kinkpairs, where the two individual kinks of a kinkpair lie on two adjacent glide planes instead of being on a single glide plane.

The 3D mode of thermally activated dislocation motion by the nucleation of kinkpairs at high/room temperatures is also in contrast with the 2D picture of dislocation motion by means of split-core states as studied in previous 2D atomistic modeling (Groger et al., 2008a, 2008b; Koester et al., 2012). The 2D split-core states, when extrapolated to 3D, will correspond to the entire dislocation line with a split-core state, akin to the uniformly split-core dislocation line predicted by Mendelev-EAM (Fig. A1(b)). Such a dislocation line with a uniform split-core state is energetically unfavorable because the system energy increases linearly with the length of the dislocation line without limit. Hence, the concept of 2D mode of dislocation motion has less significance with respect to the kinetics of screw dislocations.

We next discuss the major assumptions that we have made in our work and their implications with respect to the results we have obtained in our atomistic and crystal plasticity simulations. First, the vibrational entropy associated with kinkpair nucleation was not directly considered in our estimate of dislocation mobility. The consequence is that the kinkpair activation free energy is approximated by the kinkpair activation energy from NEB calculations. This further means that we did not account for the contribution from the stress dependent entropy while computing the prefactor $\dot{\gamma}_0$. In other words, the Meyer–Neldel compensation law (Zhu et al., 2013), which would have otherwise predicted a different value for $\dot{\gamma}_0$ by incorporating the stress-dependent entropic contribution into the attempt frequency, is considered negligible in our kinkpair kinetics when the loading range is relatively small.

Our second assumption relates to the effect of crystal zero-point vibrations that has been studied recently by Proville et al. (2012). They modified the classical transition state theory by including the effect of quantized crystalline vibration

modes, and employed these to estimate the yield stress values of BCC Fe that was found to be significantly lower than those predicted by the classical transition state theory, at temperatures lower than 80 K. They also observed that, for temperatures above half the Debye temperature (which is around 480 K for BCC Fe), the quantum-corrected transition state theory approached the classical transition state theory. Since the current work considers only the temperature regime in the vicinity of room temperature (say 200–350 K), we choose to neglect the quantum corrections in our atomistic-crystal plasticity model based on the classical transition state theory.

Third, in Eq. (7) of our crystal plasticity model for computing the resolved shear stress, we have neglected any additional terms of non-glide stress accounting for the non-Schmid behavior (Bassani et al., 2001). This assumption is expected to be physically reasonable because in the room-temperature and low-stress regime, dislocation motion proceeds via kinkpair nucleation and the non-Schmid effects are likely small (Groger and Vitek, 2008). The non-Schmid effects are due to both the intrinsic twinning–antitwinning asymmetry of the BCC lattice and the extrinsic effect of stresses on the dislocation core (Chaussidon et al., 2006; Groger et al., 2008a; Koester et al., 2012). They were found to be relevant in these 2D molecular statics studies in which the stresses employed were very high, i.e., close to the Peierls stress value. But the thermally activated kinkpair nucleation can occur at much lower stresses that are typically employed in experiments, for which the additional resistance to the dislocation motion due to the non-Schmid effects become less significant. Groger and Vitek have recognized this implication in their study (Groger and Vitek, 2008) that was based on two modes of dislocation motion in the two characteristic stress–temperature regimes with different saddle-point configurations, i.e., (i) double-kink mechanism in the low-stress and high-temperature regime that was independent of non-Schmid effects; (ii) bow-out mechanism in the high-stress and low-temperature regime (Dorn and Rajnak, 1964) that was sensitive to non-Schmid factors. While we agree with their viewpoint on the non-Schmid effects, our NEB modeling reveals a consistent thermal activation mechanism that involves the formation of double superkinks whose distance is stress-dependent and does not require the division into two stress–temperature regimes with different kinds of saddle-point configurations.

5. Conclusions

The major results and conclusions from this work are summarized below.

- We have developed an atomistically informed crystal plasticity framework for BCC Fe single crystal that is in full fidelity with the atomic mechanism of thermally activated dislocation motion via kink nucleation. The nudged elastic band method was used to capture the activation pathway and evaluate the stress dependent activation parameters of kink nucleation.
- Our atomistic results demonstrated a novel *correlated* kinkpair nucleation mechanism for the thermally activated motion of a $1/2\langle 111 \rangle$ screw dislocation, which leads to a single-humped minimum energy path and a single-step activation pathway to the neighboring {110} Peierls valley. As a result, the thermal activation of a screw dislocation involves the nucleation of double superkinks, each of which consists of the leading and trailing kinkpairs, in contrast to the classical picture of simple double-kink nucleation. The superkink structure arises from the discrete 3D nature of the saddle-point state of screw dislocation motion in BCC crystals.
- Our constitutive model quantitatively predicted the orientation dependent stress–strain behavior and the temperature/ strain-rate dependence of the yield stress, both of which agreed with the experimental results in the 200–350 K temperature regime; the strong rate dependence was rationalized by the small activation volumes of nucleation of correlated kinkpairs and the resulting double superkinks.

We conclude by noting that our work provides an atomistically informed crystal plasticity framework for studying a broad class of BCC metals with the strength/rate-limited mechanism controlled by thermally activated screw dislocation motion. Furthermore, the effects of dislocation-defect interactions, which are central to the topic of irradiated materials (Patra and McDowell, 2012) and BCC alloys (Caillard, 2011), could be incorporated into our modeling framework and thus represent future research directions. Moreover, future studies will consider the atomic mechanism of screw dislocation cross slip and non-Schmid effects in BCC crystals for bridging atomistics to crystal plasticity.
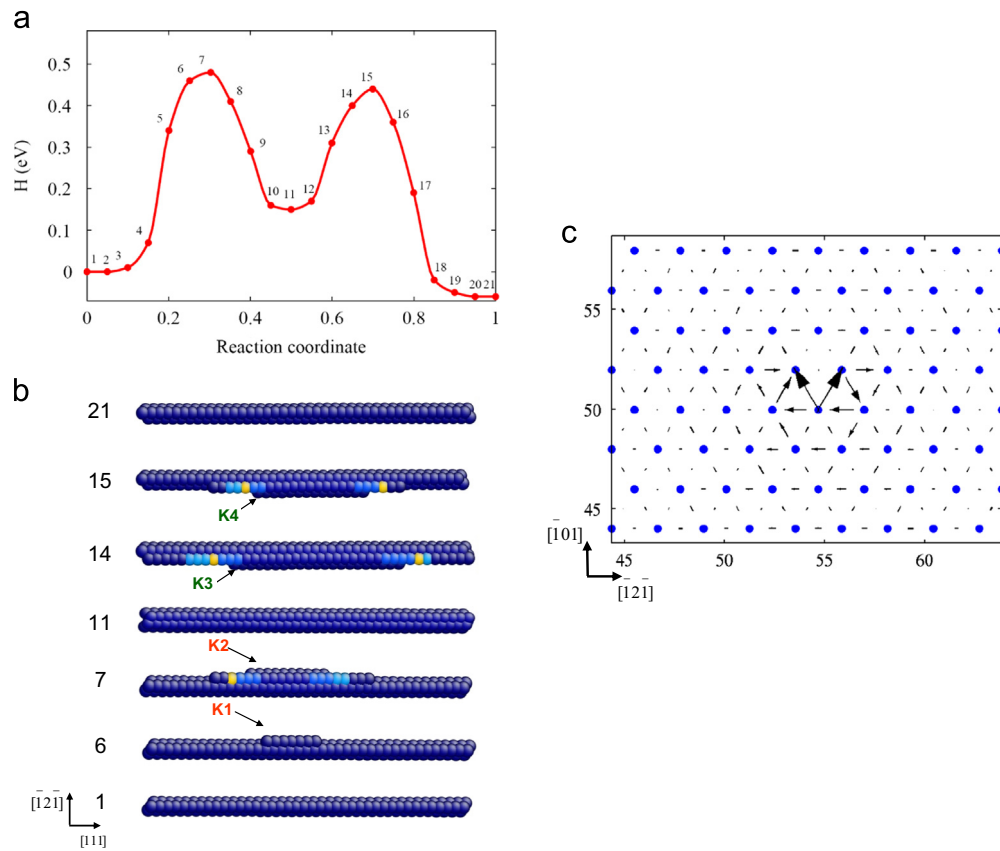
Acknowledgments

Appendix A. Uncorrelated kinkpair nucleation predicted by Mendelev-EAM

To compare with the correlated kinkpair nucleation predicted by Proville-EAM, Fig. A1 shows the minimum energy path and the atomistic details for kinkpair nucleation predicted by Mendelev-EAM at zero applied stress. The details of the figure are similar to those in Fig. 5; the kinks K1 and K2 form the leading kinkpair, and K3 and K4 form the trailing kinkpair. However, the leading and trailing kinkpairs are separated by a metastable, split-core state (replica 11) in Fig. A1(b). The two

Fig. A1. Uncorrelated kinkpair nucleation predicted by Mendelev-EAM for zero stress. (a) Double-humped minimum energy path. (b) Atomic configurations of the corresponding replicas along the minimum energy path. (c) DD plot of the split-core state of the saddle state (replica #11) in (b) .

humps on the minimum energy path (in Fig. A1(a)) denote the respective nucleation of the leading and the trailing kinkpairs, and the valley denotes the split-core state. This mode of kinkpair nucleation can be termed as the 'uncorrelated' mode, since the nucleation of the trailing kinkpair is independent of the leading one, as seen in replicas 6–11 in Fig. A1(b). The uncorrelated kinkpair mode is physically less favorable, since the system energy associated with the 2D metastable state increases linearly with the length of the screw dislocation line without limit. Fig. A1(c) shows the DD plot of the split-core structure of the saddle point, which is comparable to the short split-core segment in the correlated mode saddle state (predicted by Proville-EAM), represented by point (d) in Fig. 6(a).

References

Ackland, G.J., Bacon, D.J., Calder, A.F., Harry, T., 1997. Computer simulation of point defect properties in dilute Fe–Cu alloy using a many-body interatomic potential. Philos. Mag. A 75, 713–732.

Argon, A.S., 2008. Strengthening Mechanisms in Crystal Plasticity. Oxford Unversity Press Inc., New York.

Asaro, R.J., Needleman, A., 1985. Overview no. 42 texture development and strain hardening in rate dependent polycrystals. Acta Metall. 33, 923–953.

Bassani, J.L., Ito, K., Vitek, V., 2001. Complex macroscopic plastic flow arising from non-planar dislocation core structures. Mater. Sci. Eng. A 319, 97–101.

Brunner, D., Diehl, J., 1991. Strain-rate and temperature-dependence of the tensile flow-stress of high-purity alpha-iron above 250 K (regime I) studied by means of stress–relaxation tests. Phys. Status Solidi A 124, 155–170.

Bulatov, V.V., Yip, S., Argon, A.S., 1995. Atomic modes of dislocation mobility in silicon. Philos. Mag. A 72, 453–496.

Caillard, D., 2010. Kinetics of dislocations in pure Fe. Part II. In situ straining experiments at low temperature. Acta Mater. 58, 3504–3515.

Caillard, D., 2011. An in situ study of hardening and softening of iron by carbon interstitials. Acta Mater. 59, 4974–4989.

Chaussidon, J., Fivel, M., Rodney, D., 2006. The glide of screw dislocations in bcc Fe: atomistic static and dynamic simulations. Acta Mater. 54, 3407–3416.

Chen, Z.M., Mrovec, M., Gumbsch, P., 2013. Atomistic aspects of 1/2⟨111⟩screw dislocation behavior in alpha-iron and the derivation of microscopic yield criterion. Model. Simul. Mater. Sci. Eng. 21, 055023.

Conrad, H., 1960. Effect of temperature on yield and flow stress of Bcc metals. Philos. Mag. 5, 745–751.

Domain, C., Monnet, G., 2005. Simulation of screw dislocation motion in iron by molecular dynamics simulations. Phys. Rev. Lett. 95, 215506.

Dorn, J.E., Rajnak, S., 1964. Nucleation of kink Pairs+Peierls mechanism of plastic deformation. Trans. Metall. Soc. AIME 230, 1052.

Gilbert, M.R., Queyreau, S., Marian, J., 2011. Stress and temperature dependence of screw dislocation mobility in alpha-Fe by molecular dynamics. Phys. Rev. B 84, 174103.

Gordon, P.A., Neeraj, T., Li, Y., Li, J., 2010. Screw dislocation mobility in BCC metals: the role of the compact core on double-kink nucleation. Model. Simul. Mater. Sci. Eng. 18, 085008.

Gordon, P.A., Neeraj, T., Mendelev, M.I., 2011. Screw dislocation mobility in BCC Metals: a refined potential description for alpha-Fe. Philos. Mag. 91, 3931–3945.

Groger, R., Bailey, A.G., Vitek, V., 2008a. Multiscale modeling of plastic deformation of molybdenum and tungsten: I. Atomistic studies of the core structure and glide of $1/2\langle 111\rangle$ screw dislocations at 0 K. Acta Mater. 56, 5401–5411.

Groger, R., Racherla, V., Bassani, J.L., Vitek, V., 2008b. Multiscale modeling of plastic deformation of molybdenum and tungsten: II. Yield criterion for single crystals based on atomistic studies of glide of $1/2\langle 111\rangle$ screw dislocations. Acta Mater. 56, 5412–5425.

Groger, R., Vitek, V., 2007. Explanation of the discrepancy between the measured and atomistically calculated yield stresses in body-centred cubic metals. Philos. Mag. Lett. 87, 113–120.

Groger, R., Vitek, V., 2008. Multiscale modeling of plastic deformation of molybdenum and tungsten: III. Effects of temperature and plastic strain rate. Acta Mater. 56, 5426–5439.

Henkelman, G., Uberuaga, B.P., Jonsson, H., 2000. A climbing image nudged elastic band method for finding saddle points and minimum energy paths. J. Chem. Phys. 113, 9901–9904.

Hill, T.L., 1986. An Introduction to Statistical Thermodynamics. Dover, New York.

Johnson, R.A., Oh, D.J., 1989. Analytic embedded atom method model for Bcc metals. J. Mater. Res. 4, 1195–1201.

Jonsson, H., G. Mills, K. W. Jacobsen, 1998. Nudged elastic band method for finding minimum energy paths of transitions. In: B.J. Berne, G. Ciccotti, D.F. Coker, (Eds.), Classical and Quantum Dynamics in Condensed Phase Simulations, pp. 385–404.

Kalidindi, S.R., Bronkhorst, C.A., Anand, L., 1992. Crystallographic texture evolution in bulk deformation processing of fcc metals. J. Mech. Phys. Solids 40, 537–569.

Kang, K., Bulatov, V.V., Cai, W., 2012. Singular orientations and faceted motion of dislocations in body-centered cubic crystals. Proc. Natl. Acad. Sci. USA 109, 15174–15178.

Keh, A.S., 1965. Work hardening and deformation sub-structure in iron single crystals deformed in tension at 298 degrees K. Philos. Mag. 12, 9–30.

Kocks, U.F., Argon, A.S., Ashby, M.F., 1975. Thermodynamics and kinetics of slip. Prog. Mater. Sci. 19, 1–281.

Koester, A., Ma, A.X., Hartmaier, A., 2012. Atomistically informed crystal plasticity model for body-centered cubic iron. Acta Mater. 60, 3894–3901.

Kothari, M., Anand, L., 1998. Elasto-viscoplastic constitutive equations for polycrystalline metals: applications to tantalum. J. Mech. Phys. Solids 46, 51–83.

Kuramoto, E., Aono, Y., Kitajima, K., 1979. Thermally activated slip deformation of high-purity iron single-crystals between 4.2 K and 300 K. Scr. Metall. Mater. 13, 1039–1042.

Li, J., 2003. AtomEye: an efficient atomistic configuration viewer. Model. Simul. Mater. Sci. Eng. 11, 173–177.

Mendelev, M.I., Han, S., Srolovitz, D.J., Ackland, G.J., Sun, D.Y., Asta, M., 2003. Development of new interatomic potentials appropriate for crystalline and liquid iron. Philos. Mag. 83, 3977–3994.

Ngan, A.H.W., Wen, M., 2002. Atomistic simulation of energetics of motion of screw dislocations in bcc Fe at finite temperatures. Comput. Mater. Sci. 23, 139–145.

Patra, A., McDowell, D.L., 2012. Crystal plasticity-based constitutive modelling of irradiated bcc structures. Philos. Mag. 92, 861–887.

Plimpton, S., 1995. Fast parallel algorithms for short-range molecular-dynamics. J. Comput. Phys. 117, 1–19.

Proville, L., Rodney, D., Marinica, M.C., 2012. Quantum effect on thermally activated glide of dislocations. Nat. Mater. 11, 845–849.

Seeger, A., 1956. On the theory of the low-temperature internal friction peak observed in metals. Philos Mag. 1, 651–662.

Seeger, A., 2001. Why anomalous slip in body-centred cubic metals? Mater. Sci. Eng. A 319, 254–260.

Suzuki, H., 1968. Motion of dislocations in body-centered cubic crystals. In: Rosenfeld, A.R., Hahn, G.T., Bement, A.L., Jaffee, R.I. (Eds.), Dislocat. Dyn.. McGraw-Hill, New York, pp. 679.

Tang, M., Kubin, L.P., Canova, G.R., 1998. Dislocation mobility and the mechanical response of BCC single crystals: a mesoscopic approach. Acta Mater. 46, 3221–3235.

Ventelon, L., Willaime, F., 2007. Core structure and Peierls potential of screw dislocations in alpha-Fe from first principles: cluster versus dipole approaches. J. Comput. Aided Mater. 14, 85–94.

Vineyard, G.H., 1957. Frequency factors and isotope effects in solid state rate processes. J. Phys. Chem. Solids 3, 121–127.

Vitek, V., 2004. Core structure of screw dislocations in body-centred cubic metals: relation to symmetry and interatomic bonding. Philos. Mag. 84, 415–428.

Vitek, V., 2008. Non-planar dislocation cores: a ubiquitous phenomenon affecting mechanical properties of crystalline materials. In: Hirth, J.P. (Ed.), Dislocations in Solids. North-Holland, Amsterdam, pp. 441–514.

Wei, Q., Cheng, S., Ramesh, K.T., Ma, E., 2004. Effect of nanocrystalline and ultrafine grain sizes on the strain rate sensitivity and activation volume: fcc versus bcc metals. Mater. Sci. Eng. A. 381, 71–79.

Weinberger, C.R., Battaile, C.C., Buchheit, T.E., Holm, E.A., 2012. Incorporating atomistic data of lattice friction into BCC crystal plasticity models. Int. J. Plast. 37, 16–30.

Weinberger, C.R., Boyce, B.L., Battaile, C.C., 2013a. Slip planes in bcc transition metals. Int. Mater. Rev. 58, 296–314.

Weinberger, C.R., Tucker, G.J., Foiles, S.M., 2013b. Peierls potential of screw dislocations in bcc transition metals: predictions from density functional theory. Phys. Rev. B 87, 054114.

Yalcinkaya, T., Brekelmans, W.A.M., Geers, M.G.D., 2008. BCC single crystal plasticity modeling and its experimental identification. Model. Simul. Mater. Sci. Eng. 16, 085007.

Zhu, T., Li, J., 2010. Ultra-strength Materials. Prog. Mater. Sci. 55, 710–757.

Zhu, T., Li, J., Lin, X., Yip, S., 2005. Stress-dependent molecular pathways of silica-water reaction. J. Mech. Phys. Solids 53, 1597–1623.

Zhu, T., Li, J., Samanta, A., Kim, H.G., Suresh, S., 2007. Interfacial plasticity governs strain rate sensitivity and ductility in nanostructured metals. Proc. Natl. Acad. Sci. USA 104, 3031–3036.

Zhu, T., Li, J., Samanta, A., Leach, A., Gall, K., 2008. Temperature and strain-rate dependence of surface dislocation nucleation. Phys. Rev. Lett. 100, 025502.

Zhu, T., Li, J., Yip, S., 2004. Atomistic study of dislocation loop emission from a crack tip. Phys. Rev. Lett. 93, 025503.

Zhu, T., Li, J., Yip, S., 2013. Atomistic reaction pathway sampling: the nudged elastic band method and nanomechanics applications. In: Espinosa, H.D., Bao, G. (Eds.), Nano and Cell Mechanics. John Wiley & Sons West Sussex, UK, pp. 313–338.